Article (refereed) - postprint

Poyatos, Rafael; Heinemeyer, Andreas; Ineson, Phil; Evans, Jonathan G.; Ward, Helen C.; Huntley, Brian; Baxter, Robert. 2014. **Environmental and vegetation drivers of seasonal CO2 fluxes in a sub-arctic forest–mire ecotone.** *Ecosystems*, 17 (3). 377-393. https://doi.org/10.1007/s10021-013-9728-2

Environmental and vegetation drivers of seasonal CO_2 fluxes in a sub-Arctic forest-mire ecotone

Rafael Poyatos [*a, b], Andreas Heinemeyer [c], Phil Ineson [c], Jonathan G. Evans [d], Helen C. Ward [d], Brian Huntley [b] and Robert Baxter [b]

[a] CREAF, Cerdanyola del Vallès 08193, Spain

[b] School of Biological and Biomedical Sciences, Durham University, Durham DH1 3LE, UK.

[c] Environment Department, Stockholm Environment Institute, University of York, York YO10 5DD, UK

[d] Centre for Ecology and Hydrology, Wallingford, Oxfordshire, UK

[*]Corresponding author: r.poyatos@creaf.uab.es

Short title: CO_2fluxes in a sub-Arctic forest-mire ecotone

R.P. conceived and designed the study, performed research, analysed data and wrote the paper; A.H conceived and designed the study and revised the paper; P. I conceived and designed the study and revised the paper; J.G.E. performed research, analysed data and revised the paper; H.C.W performed research, analysed data and revised the paper; B.H. conceived and designed the study and revised the paper; R.B. conceived and designed the study and revised the paper;

Abstract

Unravelling the role of structural and environmental drivers of gross primary productivity (GPP) and ecosystem respiration (R_{eco}) in highly heterogeneous tundra is a major challenge for the upscaling of chamber-based CO_2 fluxes in Arctic landscapes. In a mountain birch woodland-mire ecotone, we investigated the role of LAI (and NDVI), environmental factors (microclimate, soil moisture) and microsite type across tundra shrub plots (wet hummocks, dry hummocks, dry hollows) and lichen hummocks, in controlling net ecosystem CO_2 exchange (NEE). During a growing season, we measured NEE fluxes continuously, with closed dynamic chambers, and performed multiple fits (one for each three-day period) of a simple light and temperature response model to hourly NEE data. Tundra shrub plots were largely CO_2 sinks, as opposed to lichen plots, although fluxes were highly variable within microsite type. For tundra shrub plots, microsite type did not influence photosynthetic parameters but it affected basal (i.e., temperature-normalised) ecosystem respiration (R_0). PAR-normalised photosynthesis (P_{600}) increased with air temperature and declined with increasing vapour pressure deficit. R_0 declined with soil moisture and showed an apparent increase with temperature, which may underlie a tight link between GPP and R_{eco}. NDVI was a good proxy for LAI, maximum P_{600} and maximum R_0 of shrub plots. Cumulative CO_2 fluxes were strongly correlated with LAI (NDVI) but we observed a comparatively low GPP/LAI in dry hummocks. Our results broadly agree with the reported functional convergence across tundra vegetation, but here we show that the role of decreased productivity in transition zones and the influence of temperature and water balance on seasonal CO_2 fluxes in sub-Arctic forest-mire ecotones cannot be overlooked.

Key-words: carbon balance, ecosystem respiration, gross primary productivity, leaf area index, lichen, NDVI, net ecosystem exchange, soil moisture, transition zones, tundra

Introduction

Arctic mires and tundra ecosystems store large amounts of C (Turunen and others, 2002; Limpens and others, 2008) and are experiencing shifts towards more productive vegetation as climate at high-latitudes becomes warmer (Beck and others, 2011; Elmendorf and others, 2012). Climate-driven shifts in net ecosystem CO_2 exchange (NEE) of Arctic tundra are highly relevant for carbon-climate feedbacks at the global scale, especially under the enhanced warming predicted for the Arctic (Christensen and others, 2007). On one hand, warmer conditions may enhance gross primary productivity (GPP) through the alleviation of thermal constraints on photosynthesis, changes in species composition and/or the increase of growing season length and nutrient availability (Natali and others, 2012). On the other hand, higher temperatures and associated hydrological changes may increase ecosystem respiration (R_{eco}) (Dorrepaal and others, 2009) and even release old C stored in permafrost soil and peat (Schuur and others, 2009), potentially offsetting any productivity increases.

Annual sums of ecosystem CO_2 fluxes have shown that NEE is typically negative (i.e. net C uptake by the ecosystem) in northern mires (Lund and others, 2010). During warm and dry years, however, sink strength generally decreases and mires can turn into

net carbon sources (Alm and others, 1999) because of increases in R_{eco}, declines in GPP, or both (Moore and others, 2002; Bubier and others, 2003). Hence, the relative sensitivities of GPP and R_{eco} to temperature, growing season length and substrate water content will determine the climate-induced changes in NEE of high latitude mires and tundra ecosystems. These responses will likely vary across ecosystem types, moisture gradients and microtopographic positions (Oberbauer and others, 2007), which can vary considerably on spatial scales of meters or less in spatially complex Arctic landscapes (Asner and others, 2003; Spadavecchia and others, 2008).

This heterogeneity of high-latitude low-stature vegetation results in a marked spatial variability of NEE and its flux components associated to microtopography, local hydrology (Heikkinen and others, 2004; Nobrega & Grogan, 2008; Pelletier and others, 2011) and community composition (Riutta and others, 2007). However, functional convergence of canopy N-use across Arctic vegetation types (Van Wijk and others, 2005) results in GPP being largely explained by microclimate and leaf area index (LAI) alone (Shaver and others, 2007; Street and others, 2007). In these ecosystems, the observed normalised difference vegetation index (NDVI), a good surrogate of LAI, and hence of GPP at given environmental conditions, is often also a good predictor of measured R_{eco} (McMichael, 1999; Boelman and others, 2003). However, whether these relationships between LAI (NDVI) and CO_2 exchange also hold for integrated fluxes over the entire growing season has not been thoroughly tested (but see Marushchak and others (2013)).

Landscape-level studies of CO_2 fluxes in tundra and mire ecosystems depict a pronounced seasonal variability in NEE and its components (Lindroth and others, 2007; Lund and others, 2010). At a finer spatial scale, seasonal variation in CO_2 fluxes is high (Bubier and others, 2003) and responses to environmental drivers may be ecosystem-specific (Nobrega & Grogan, 2008). Because of this high spatial and temporal variability, detailed measurements across time at multiple points in space are critical for understanding the magnitude and variability of CO_2 exchange in different vegetation and ecosystem types for point-to-landscape scaling efforts (Stoy and others, 2013; Oechel and others, 1998; Soegaard and others, 2000).

The margins of mires at the mountain birch *(Betula pubescens* ssp. *czerepanovii* (Orlova) Hamet-Ahti) woodland-tundra ecotone in northern Fennoscandia are highly representative of heterogeneous low-arctic vegetation. Here, the formation of cryogenic earth hummocks results in a complex microtopography and thus a variety of habitats that differ in snow cover during the winter and substrate moisture during the growing season (Van Vliet-Lanoe & Seppala, 2002). In this study, we used an automated chamber system to measure hourly NEE across a mire-mountain birch woodland ecotone in northern Finland. We focused on differences on NEE controls across four microsites: three tundra shrub microsites, differing in microtopographic position and soil moisture, and one lichen microsite. Fluxes were modelled using semi-empirical responses to light and temperature, yielding normalised GPP at PAR=600 µmol m^{-2} s^{-1} (P_{600}) and R_{eco} normalised to an air temperature of 0°C (basal ecosystem respiration, R_0). These and other parameters associated with diel environmental controls on NEE

were analysed in relation to seasonal variation in environmental drivers (mainly microclimate and soil moisture) and plant structure obtained from LAI harvests and seasonal hand-held NDVI measurements. We hypothesised that: (H1a) NDVI would be a good surrogate for LAI and (H1b) would explain differences in P_{600} across microsites. It was also postulated that (H2) for tundra shrub microsites, seasonality in photosynthetic parameters would be unaffected by microsite type and would be largely explained by NDVI and air temperature (H3a). We also hypothesised that R_0 would be positively related to NDVI and, given the prevailing wet conditions in sub-Arctic mires, R_0 would decline with soil moisture because of limited oxygen diffusion into the soil (H3b). According to the functional convergence reported for tundra vegetation (H4) growing season cumulative NEE would be strongly correlated with LAI (or NDVI) across microsites.

Methods

Study site and plot characteristics

The study area (69°29'35.37"N, 27°13'52.91"E, 272 m.a.s.l.) was located near Petsikko, *ca.* 35 km south of the Kevo Subarctic Research Institute in northern Finland. Mean annual temperature at Kevo (80 m.a.s.l.) is -1.6 ºC and annual precipitation is 415 mm (1962-2007, Kevo Subarctic Research Institute). The mineral soil is formed by glacial till and underlain by gneiss. The site presents topographical depressions occupied by open water, gradually turning to *Eriophorum-Carex* lawns and *Sphagnum* pools at the

mire (peatland) margins. The surrounding gentle slopes are mostly covered by mesic tundra shrubs growing on peat deposits, grading into a sparse mountain birch (*Betula pubescens ssp. czerepanovii)* woodland.

We studied a forest-mire ecotone (Appendix 1 in Online publication), characterised by hummocks with a typical height of *ca* 0.6 m and a maximum diameter of *ca*. 1 m. The mean depth of the organic horizon was *ca.* 20 cm (Wayolle, 2011). Ecotones between mires and sub-Arctic woodland in northern Fennoscandia display characteristic formations of peat hummocks, associated with the area of discontinuous permafrost (Van Vliet-Lanoe & Seppala, 2002). Even though there is no permafrost at the site, these hummocks can show ice lenses in their cores even in late summer (Wayolle, 2011) and are usually covered by various shrubs, mosses and lichens. The shrubs were dominated by mesic tundra heath species, such as *Empetrum nigrum* L., *Vaccinium vitis-idaea* L., *Calluna vulgaris* L. (Hull) and *Vaccinium myrtillus* L. The moss species included *Sphagnum fuscum* (Schimp.) Klinggr., *Pleurozium schreberi* (Brid.) Mitt., and acrocarpous mosses. The lichens (*Cetraria* spp. and *Cladonia* spp.) form a thin cryptogamic crust covering tall hummock tops devoid of vascular vegetation because of frost exposure and wind abrasion (Van Vliet-Lanoe & Seppala, 2002).

We deployed 12 PVC collars (19.9 cm internal diameter and 4.5 cm height) in early June 2008 to measure four microsite types, with three replicates for each type (Table 1). Three microsite types were dominated by tundra shrubs and differed in their spatial location, both in terms of microtopography and position along the mire to forest

ecotone: mire hummocks (HM) were located close to the wetland and forest hummocks (HF) were nearer the forest edge and dry hollows (DH) occupied depressions at intermediate locations. HM and HF were dominated by *E. nigrum* and *Vaccinium* species, and DH was almost exclusively covered by *C. vulgaris*. Lichen hummocks (HL) had only a poor lichen and moss cover (Table 1). Given their similar shrub vegetation characteristics, HM, HF and DH microsites will hereafter be referred to as 'tundra shrub microsites' throughout the manuscript.

Multiplexed automated CO_2 flux measuring system

We used a closed dynamic CO_2 flux system for measuring CO_2 flux rates (μmol CO_2 m^{-2} s^{-1}). The system comprised an infra-red gas analyser (Li-Cor 8100, Li-Cor Inc., Lincoln, Nebraska, USA), a custom-built multiplexed gas handler unit (Electronics Workshop, Biology Department, University of York, UK) and 12 clear, Perspex chambers based on a commercial soil respiration model (LiCor 8100-101; 20 cm diameter). Chambers closed and opened sequentially, allowing hourly measurement cycles of 12 vegetation patches at a maximum radial distance of 20 m from the multiplexer. The chamber bases had rims with a rubber gasket, which ensured a tight fit with PVC collars. These collars were deployed on the 12 selected patches and gently sealed to the ground, without cutting or inserting into the substrate, using non-setting plumber's putty (Plumber's Mait, Bostik Ltd., Leicester, UK). We took this precaution to avoid damaging the prostrate stems and the roots of dwarf-shrub tundra species, which could potentially affect measured C fluxes as shown for another peatland

(Heinemeyer and others, 2011). The system operated from the 11th of June (DOY 163) until the 14th of September (DOY 258) of 2008. Further details on the operation of a similar system used for respiration measurements can be found in Heinemeyer and others (2011).

We used the meteorological sign convention for NEE, in which a net flux from the atmosphere to the biosphere is negative. NEE was calculated as:

$$NEE = -\frac{PV}{ART_0}\frac{d}{dt}[CO_2]_{dry} \qquad \text{Eq. 1}$$

where P is air pressure inside the chamber (Pa), V (m^3) is the system volume in (chamber, irga/multiplexer and tubing), T_0 (°C) is air temperature at chamber closure, R (J K^{-1}µmol^{-1}) is the ideal gas constant, A is chamber surface area (m^2) and $d[CO_2]_{dry}/dt$ (µmol mol^{-1} s^{-1}) is the rate of change in water vapour-corrected CO_2 concentration in the chamber headspace. We calculated this rate from CO_2 and water vapour concentrations measured every 2 seconds, over the 150 s period when the chamber remained closed. We estimated $d[CO_2]_{dry}/dt$ from the first order term of a quadratic fit between $[CO_2]_{dry}$ and time since chamber closure. Nonlinear fits describe better the concentration dynamics in the closed chamber, and do not systematically underestimate the fluxes (Kutzbach and others, 2007). However, in the presence of noisy concentration data under low flux conditions, we opted for the more stable linear fit; we selected the linear regression whenever the slope for the linear fit and the linear term of the quadratic fit had opposite signs.

208 *Vegetation and structural measurements*

209

210 We took pictures of all the plots with a digital camera (DX 7630, Eastman Kodak,
211 Rochester, NY, USA) on the 31st of July 2008, and estimated percentage cover for each
212 species combining manual delimitation with the 'selection by colour' tool in the image
213 analysis software GIMP v. 2.4.6. At the end of the flux measurement period (16th of
214 September), we harvested all the aboveground biomass inside the collars, dried it for 48
215 h at 60ºC and weighed it. Leaf biomass for each plot was converted into leaf area using
216 specific leaf area (SLA) measured for each species in nearby plots (Fletcher, Sloan &
217 Phoenix, unpublished), summed up and calculated plot-scale LAI (Table 1).

218

219 We measured NDVI on the study plots on seven dates (29th June, 2nd July, 31st July, 8th
220 August, 1st September, 6th September, and 11th September). We used a two-channel
221 sensor (SKR 1800, Skye Instruments) attached to a hand-held console (SpectroSense2,
222 Skye Instruments) to measure surface reflectance in the red (channel 1, 0.56-0.58 nm)
223 and near-infrared (channel 2: 0.725-1.1 nm) bands. We held the sensor pair at a height
224 of 0.4 m above the plot, so that the effective area measured by the sensor measuring
225 reflected light (25º field of view, no diffuser cap attached) corresponded to the collar
226 area. We used the diffuser cap to cosine-correct the incident light measured by the
227 upward-looking sensor. NDVI was linearly interpolated across measuring dates in order
228 to obtain a continuous daily estimate. For our plots, dominated by evergreen species
229 (Table 1), this interpolation was a reasonable approximation after checking NDVI
230 variation measured from a nearby tower-mounted sensor (J. Evans, unpublished results).

Environmental measurements

We measured photosynthetically active radiation (PAR) with a pair of quantum sensors (Delta-T, Burwell, UK); one was deployed inside one of the collars and the other just outside the same collar. We thus quantified a *ca.* 20% PAR attenuation during chamber closure by fitting a power function between ambient and inside-chamber PAR ($PAR_{ambient}=0.80 \cdot PAR_{chamber}^{1.01}$; $R^2=0.97$; $N=945$). We used this function to correct ambient PAR to inside-chamber values (needed to correct for ambient NEE fluxes).

We obtained plot-specific air temperature from the value measured by chamber thermistors at chamber closure. We calculated vapour pressure deficit (VPD) using air temperature and relative humidity in the chamber (Jones, 1992). Site air temperature, PAR and precipitation were measured in a meteorological tower at *ca.* 50 m from the location of the chambers. We measured half-hourly volumetric soil moisture (SWC; CS616 water content reflectometer and CR1000 datalogger, Campbell Scientific, UK) in one representative plot of each vegetation type (N=4). We installed the reflectometer rods (30 cm long) obliquely so that the measurement was representative of a larger area; measuring depth was thus 0-10 cm. We also measured soil temperature (5 cm depth) (every 30 min) in all plots by soil thermistors connected to a datalogger (DL2e, Delta-T Devices, Cambridge, UK).

NEE modelling

We modelled plot-scale CO_2 fluxes using semi-empirical responses to light and temperature. We binned hourly daytime NEE fluxes in 3-day classes and fitted the following model, which combines a rectangular hyperbola to simulate GPP and an exponential relationship between ecosystem respiration and temperature (Williams and others, 2006):

$$NEE = R_0 e^{\beta T} - \frac{P_{max} PAR}{k + PAR} \qquad \text{Eq. 2}$$

Where R_0 is basal respiration (μmol CO_2 m^{-2} s^{-1}), representing ecosystem respiration at 0 °C, β (°C^{-1}) is respiration sensitivity to temperature, P_{max} (μmol CO_2 m^{-2} s^{-1}) is asymptotic maximum photosynthesis and k is the half-saturation constant (μmol PAR m^{-2} s^{-1}). For comparative purposes, we calculated gross photosynthesis at PAR = 600 μmol m^{-2} s^{-1} (P_{600}) (Street and others, 2007), we expressed respiration sensitivity to temperature as a Q_{10} coefficient ($Q_{10}=e^{\beta}$) and we converted k to quantum efficiency ($\alpha = P_{max}/k$; μmol CO_2 μmol^{-1} PAR) (Atkin and others, 2005; Street and others, 2007).

Despite some gaps due to power failures in this remote and harsh environment, we obtained CO_2 time series that covered 51-58% of the hourly intervals within the measuring period, depending on the plot (*cf.* Results). Therefore, the parameters of the NEE model were linearly interpolated to complete missing days and then the model was

applied to gap-fill the NEE time series. The same model was also used to decompose NEE into GPP and R_{eco}. The completed CO_2 flux time series were then aggregated into growing season cumulative values.

Data analyses

All data analyses, including CO_2 flux calculations, were carried out using the statistical package R 2.9 (R Development Core Team, 2009). We calculated the 5% and 95% quantiles of NEE hourly rates ($NEE_{5\%}$ and $NEE_{95\%}$, respectively) for each plot, to represent robust estimates of sustained, maximum CO_2 uptake and release capacity and to aid in comparative analyses across vegetation types. Linear mixed-effects models (Pinheiro & Bates, 2000) were used to analyse the influences of environmental drivers and structural variables on the seasonal dynamics of NEE model parameters. Models were fitted using restricted maximum likelihood (package lme, R 2.9), with plot code introduced as a random factor. We tested all possible combinations of time (DOY), environmental drivers (air temperature, VPD and soil moisture) and structural variables (NDVI, vegetation type) as fixed effects. As the NEE model parameters are subject to temporal autocorrelation we introduced a correlation structure based on a continuous first-order autoregressive process (corCAR1). Model performance was assessed via graphical inspection of the residuals and their autocorrelation function. Models with the lowest Akaike's Information Criterion (AIC) were retained and R^2 values were calculated using likelihood ratio tests (lmR2LR, package lmmfit, v. 1.0).

Results

299

300 *Meteorology and soil moisture during the growing season*

301

302 Daily mean air temperatures were close to 0 ºC at the beginning and the end of the study
303 period, and only reached maximum values of 15 ºC (Figure 1a). June-August average
304 temperature was 8.4 ºC, cooler than the altitude-corrected climatic value (1962-2007,
305 9.9 ºC). Precipitation (167.5 mm, June-August average) was evenly distributed
306 throughout the study period (Figure 1c), and almost identical to the climatic average
307 (171 mm). Daily radiation input decreased from values of 40-50 mols m^{-2} day^{-1} in June
308 and July to values of *ca.* 20 mols m^{-2} day^{-1} in August and September (Figure 1b).
309 Average soil temperature (measured at a depth of 5 cm) over the growing season was
310 9.6 ± 0.02 °C, and only forest hummocks (HF) were slightly warmer (0.07 °C, P =
311 0.033) than the overall mean. Soil water content was higher in mire hummocks (HM)
312 compared with forest hummocks (growing season mean ± SE values of 0.67 ± 0.004
313 cm^3 cm^{-3} and 0.19 ± 0.02 cm^3 cm^{-3}, respectively). Dry hollows (DH) and lichen
314 hummocks (HL) showed similar soil moisture values (0.38 ± 0.002 cm^3 cm^{-3} and 0.33 ±
315 0.002 cm^3 cm^{-3}, respectively) and dynamics throughout the growing season (Figure 1d).

316

317 *Seasonal and diel courses of NEE*

318

319 For tundra shrub microsites (i.e. HM, HF and DH), NEE displayed pronounced and very
320 similar seasonal dynamics, whereas the lichen hummocks (HL) showed much lower

fluxes, acting as carbon sources for most of the growing season (Figure 2). Although maximum hourly NEE rates peaked at -12 to -15 µmols CO_2 m^{-2} s^{-1} around DOY 220 (early August), these values were infrequent and average daytime $NEE_{5\%}$ of tundra shrub microsites was -5.2 µmols CO_2 m^{-2} s^{-1}. $NEE_{5\%}$ values for HL plots were very close to zero (-0.09 µmols CO_2 m^{-2} s^{-1}). Within tundra shrub microsites, $NEE_{5\%}$ did not vary across microsite types (P = 0.958). However, a marginally significant difference (P = 0.059) was found between night-time $NEE_{95\%}$ averaged for all tundra shrub microsites (3.02 µmols CO_2 m^{-2} s^{-1}) compared with that of HL plots (1.78 µmols CO_2 m^{-2} s^{-1}). The diel courses of NEE confirmed that within-microsite variability was the largest source of variation in NEE fluxes, especially during the peak growing season (Figure 3).

Seasonality in NEE model parameters

The NEE model performed well (Appendix 2 in Online publication) with better fits for tundra shrub microsites (average adjusted R^2 = 0.78) than for HL (average adjusted R^2 = 0.53). For all tundra shrub microsites, P_{600} showed a clear seasonal pattern, with a peak around DOY 220, regardless of the microsite type (Figure 4). Across microsites, quantum efficiency (α) tended to show similar increases at the beginning of the growing season. However, the late season decline in α was not as fast as the early season rise, especially for DH plots, which showed a broad mid-season plateau in the value of α (Figure 4). HL plots showed much lower values for P_{600} and α, representing only 16% and 27%, respectively, of the average values obtained for tundra shrub microsites. Basal respiration also showed peaked dynamics (peak between DOY 195 and 220), although

not as clear as that observed for P_{600}. One of the HL plots (HL1) had R_0 values of similar magnitude to those of the tundra shrub plots. The Q_{10} coefficient showed a slightly bimodal pattern, with higher values during early and peak season (Figure 4). Again, higher variability in the parameters of the NEE model was found within microsites compared to that observed among microsites (Figure 4).

NDVI and environmental variables drive NEE seasonality

The highest NDVI values were observed for HF plots, HL showed the lowest (Figure 4) and HM and DH displayed intermediate NDVI. Although both microsite type (F = 12.04, $d.f.$ = 8, P = 0.0025) and date (F = 5.67, $d.f.$ = 68, P = 0.0201) had an effect on NDVI values, repeating the analysis omitting the HL plots showed that only date remained as a significant effect on NDVI of tundra shrub plots (F = 9.20, $d.f.$ =51, P = 0.0038) and microsite type played no role (F = 2.28, df = 6, P = 0.1830). Accordingly, the peak value of NDVI showed a tight correlation with both plot vascular biomass and LAI (Figure 5c,d, Table 2). Similarly, maximum NDVI was strongly related to peak P_{600} and R_0 values (Figure 5a,b, Table 2). However, some discrepancy was observed, as the seasonal course of NDVI showed an early season increase but a very slight late season decline, compared to P_{600} dynamics (Figure 4).

NDVI and air temperature emerged as the main variables controlling the NEE model parameters for tundra shrub microsites, albeit NDVI was only marginally significant in

366 the R_0 model (Table 3). A quadratic effect of air temperature and a negative effect of
367 VPD were found for P_{600}. A negative influence of SWC was observed for R_0 but not for
368 the Q_{10} coefficient; this latter parameter only varied with DOY (Table 3). No effect of
369 microsite type was observed on P_{600} or α, but R_0 did vary across microsites (Table 3),
370 However, this microsite effect was highly correlated with the SWC effects (r > 0.97;
371 data not shown).

372

373 *Environmental and structural controls on growing season CO_2 fluxes*

374

375 Variability in growing season CO_2 fluxes was high within microsite types (Figure 6)
376 and the only consistent differences were found between tundra shrub and lichen
377 microsites (Table 4). Within-microsite variability was less for R_{eco} than for GPP (Table
378 4). Lichen-covered plots were a consistent C source whereas tundra shrub plots were C
379 sinks, except for plot HF1 (Figure 6, Table 4). There were large, although only
380 marginally significant, differences in NEE and GPP/LAI between HM and HF
381 microsites, with much higher C uptake per unit leaf area in HM microsites (Table 4).
382 We also found that both LAI and NDVI were good predictors of growing season NEE,
383 GPP and R_{eco} across plots (Figure 7, Table 2) and that R_{eco} was strongly related to GPP
384 in a nonlinear fashion (Figure 8, Table 2).

385

386 **Discussion**

387

388 *Vegetation parameters and instantaneous NEE fluxes*

389

390 Within the studied ecotone, between mire and forest, we observed a great variability in
391 LAI and vascular biomass of tundra shrub and lichen hummocks, characteristic of sub-
392 Arctic areas. NDVI values were tightly related to biomass and LAI across plots,
393 consistent with our hypothesis H1a and with findings for other tundra ecosystems
394 (Boelman and others, 2005; Street and others, 2007). Accordingly, maximum NDVI
395 varied from very low values for HL plots, which were close to pre-growing season,
396 baseline values (≈0.3) (Huemmrich and others, 2010), to typical maximum NDVI
397 observed in sub-Arctic heath (Street and others, 2007). Seasonal variation of NDVI was
398 also in agreement with that measured in other Arctic ecosystems (La Puma and others,
399 2007; Huemmrich and others, 2010).

400

401 Our results showed slightly lower instantaneous NEE fluxes compared to other studies
402 using automated chambers in northern peatlands (Bubier and others, 2003; Burrows and
403 others, 2005), probably because of lower latitudes and thus milder climatic conditions in
404 these other studies. The length of the sink period was consistent with recent syntheses of
405 eddy flux studies showing that sub-Arctic and Arctic mires display a shorter sink period
406 compared to other boreal peatlands (Lindroth and others, 2007; Lund and others, 2010).
407 We also observed high within-microsite variability in NEE rates, largely related to LAI
408 variations across plots, as has been reported across Arctic tundra sites (Shaver and
409 others, 2007).

410

411 *Seasonal drivers of photosynthetic parameters*

412

413 The parameters describing the response of GPP to light varied seasonally in parallel to
414 NDVI dynamics, and no differences were found amongst the different tundra shrub
415 microsites. Maximum P_{600} peaked at the end of July and started to decline in August, as
416 observed in other sub-Arctic sites (Alm and others, 1997). Maximum P_{600} was tightly
417 related with maximum NDVI across plots (H1b), but our mixed-effects models did not
418 include any interaction between vegetation type and DOY (or NDVI) to explain
419 variation in either P_{600} or α. Therefore, we could not detect any season-specific
420 differences in the response to light of leaf-area based photosynthesis in our tundra shrub
421 plots, consistent with our hypothesis H2. Similar phenological patterns of leaf area-
422 based P_{600} have also been reported across *Empetrum* and dry heath patches in sub-
423 Arctic tundra at Abisko, northern Sweden (Street and others, 2007).

424

425 Nevertheless, during the late growing season, P_{600} decreased proportionally faster in
426 comparison to NDVI, concomitant with photoperiod and air temperature decline. This
427 suggests that NDVI may not entirely capture the biochemical downregulation of
428 photosynthesis occurring in late summer. Accordingly, the mixed model results for P_{600},
429 apart from the NDVI effects, showed positive, linear and quadratic effects of
430 temperature. A positive influence of air temperature on P_{max} and on the half-saturation
431 constant of photosynthesis k (inversely proportional to α; cf. Methods), has also been
432 reported for Arctic tundra plots in Alaska (Williams and others, 2006). Moreover,
433 quadratic effects are consistent with nonlinear, delayed responses of P_{max} to

434 temperature, as shown previously for two of the species included in this study: *Calluna*
435 *vulgaris* and *Vaccinium vitis-idaea* (Kulmala and others, 2009, 2011).We have also
436 found a negative effect of VPD on P_{600} (Williams and others, 2006), which may be due
437 to a combination of two processes: (1) stomatal limitations on CO_2 assimilation or (2)
438 desiccation-induced reductions in moss photosynthesis. Although we did not find an
439 effect of soil moisture on $P_{600,}$ as other studies suggest (Kulmala and others, 2011),
440 atmospheric drought alone may induce stomatal closure in some Arctic species
441 (Humphreys and others, 2006). In contrast, gross productivity of mosses appears to be
442 rather insensitive to water content under typical climatic conditions in similar sub-
443 Arctic locations (Street and others, 2012).

444

445 *Seasonal drivers of respiration parameters*

446

447 The seasonal variation in R_0 tracked the dynamics of NDVI and photosynthetic
448 parameters, while the Q_{10} coefficient decreased slightly throughout the growing season,
449 and did not vary with any environmental variable. These results are in agreement with
450 other chamber-based studies in peatlands (Cai and others, 2010) and the invariant,
451 intrinsic Q_{10} coefficient for R_{eco} observed at the global scale (Mahecha and others,
452 2010). We also observed positive and negative effects of air temperature and soil water
453 content, respectively, on R_0. If we assume that the NEE model absorbed the response of
454 R_{eco} to temperature in the Q_{10} coefficient, we may interpret the apparent positive effect
455 of air temperature as being mediated by recent photosynthesis. High air temperatures
456 are related to increased radiation and both enhance plant photosynthesis, which, in turn,

would boost plant respiration and stimulate respiration of labile exudates by soil microbes, hence increasing R_{eco}. This explanation would be supported by the tight link between recently assimilated carbon and R_{eco} observed in temperate heathland (Larsen and others, 2007) and Arctic tundra (Subke and others, 2012). The negative effect of soil water content on R_{eco} can be explained by low soil aeration limiting microbial decomposition (Johnson and others, 1996), especially in the moister HM microsite, close to the mire edge. Overall, these results support our hypothesis H3b but also highlight additional vegetation controls on R_{eco}.

Structural controls on growing season CO_2 fluxes across microsites

Importantly, all tundra shrub microsites were consistent CO_2 sinks compared to lichen hummocks, which were CO_2 sources. However, because of the low number of replicates, we could not find significant differences in growing season NEE across microsites. Previous studies have shown that tundra heath patches can be CO_2 sinks (Alm and others, 1997; Marushchak and others, 2013), CO_2 sources (Alm and others, 1999; Heikkinen and others, 2004) or CO_2 neutral (Nobrega & Grogan, 2008; Maanavilja and others, 2011), probably reflecting differences in LAI and specific environmental conditions. Likewise, bare peat and lichen communities are consistent CO_2 sources (Heikkinen and others, 2004; Marushchak and others, 2013).

Across plots, all growing season CO_2 fluxes were strongly and positively related to LAI,

as also recently observed in a reconstruction of seasonal CO_2 budget using manual chamber measurements (Marushchak and others, 2013). Similarly, we observed a good correspondence between peak NDVI and all the CO_2 flux components integrated over the growing season. While the link between NDVI and GPP is mechanistically straightforward, the association between NDVI and R_{eco} might be explained by a high contribution of autotrophic respiration to R_{eco} and/or a tight link between growing season R_{eco} and GPP, as we observed here. NDVI has indeed been related to instantaneous or daily GPP and R_{eco} (McMichael, 1999; Boelman and others, 2003), although sometimes with a low explanatory power (La Puma and others, 2007; Dagg & Lafleur, 2010).

Although the relationship between NDVI and NEE was weaker than for GPP and R_{eco}, NDVI still explained a high proportion of NEE variation, in contrast with the weak or non-existent relationships reported for other plot-scale studies in the Arctic (La Puma and others, 2007; Dagg & Lafleur, 2010). Our results are thus in agreement with the observed control of LAI on ecosystem-level NEE across northern peatlands and tundra sites (Lund and others, 2010). We are not aware of any other study in low Arctic ecosystems showing these strong vegetation controls on growing season NEE and its components for patch-scale CO_2 fluxes, measured at high temporal resolution over the course of an entire growing season.

Implications for CO_2 flux upscaling

504 The NEE model employed in this paper does not include LAI as an input, as the one
505 proposed by Shaver and others (2007) does. Hence, here, seasonal variation in the
506 parameters of the NEE model implicitly includes seasonal LAI dynamics and we
507 analyse a posteriori the roles of structural vs. environmental drivers in controlling NEE
508 using a mixed-effects model. We follow this approach because one of the aims of this
509 paper to test whether our data support the reported functional convergence in NEE
510 controls across Arctic ecosystems, not to test the direct applicability of the model by
511 Shaver others in our site. Moreover, there are some drawbacks to the application of this
512 model, such as the uncertainty in LAI estimation (cf. discussion in Shaver and others
513 2007).

514 Overall, our results are broadly consistent with this functional convergence, but
515 underline the additional role of air temperature and VPD effects on the seasonal light
516 response of tundra vegetation. In addition, GPP per unit leaf area in mire hummocks
517 (HM) was more than double the value observed for drier forest hummocks (HF), and
518 similar to dry hollows (DH). The similarity in GPP/LAI observed between DH and HM
519 microsites (i.e. under contrasting soil moisture conditions) would not support a
520 hypothetical effect of soil moisture in reducing GPP/LAI, although the HF microsite
521 was even drier than the DH microsite and, therefore, a drought effect could not be
522 discarded. Various studies on Arctic tundra have indeed shown increased productivity
523 in wetter patches (Nobrega & Grogan, 2008; Dagg & Lafleur, 2011) and reduced light
524 use efficiency in dry microsites (Huemmrich and others, 2010). However, a reduction in
525 GPP/LAI could be attributed to a suboptimal arrangement of vegetation within the
526 transition zone. A recent study has reported this phenomenon for ecotones containing *E.*
527 *nigrum* in another sub-Arctic site and *Betula nana*-dominated transects within the same

study area (Fletcher and others, 2012). However, whether this is the only explanation for the observed differences is doubtful, as changes in vegetation composition between HF and HM plots are minor (Table 1). Our results thus only partly support hypothesis H4 and suggest, for growing season CO_2 fluxes, a decrease in GPP/LAI within sub-Arctic ecotones from mires to forest, which may be mediated by reductions in soil moisture.

Another important implication of our results concerns the consistent CO_2 sources observed in lichen hummocks. The analysis of a land classification map obtained from airborne photography (T. Hill, unpublished) shows that *ca.* 20% of the area in the ecotone between forest and mire is covered by lichen. Therefore, these hotspots for C release will significantly contribute to reduce the C sink capacity at the landscape scale. However, poorly vegetated and bare peat hummocks usually present frozen cores (Van Vliet-Lanoe & Seppala, 2002), as observed at the study site (Wayolle, 2011), which may degrade with climate warming and result in increased net C uptake after shrub colonisation of these hummocks (Bosiö and others, 2012).

Concluding remarks

Our results showed a great variability in NEE fluxes within tundra shrub and lichen microsites at diel and seasonal timescales, which could be largely explained by microclimate and LAI. Given the good correspondence observed between vegetation

parameters and NDVI, this spectral index was found to be a good predictor of both maximum photosynthetic and respiratory potential. Other studies on low-stature vegetation have shown that broad-band NDVI can be used to predict NEE light response parameters (Wohlfahrt and others, 2010). Nevertheless, we have also found that other environmental drivers modulate the dynamics of vegetation controls on CO_2 fluxes, and they should therefore be included in models of NEE in low Arctic ecosystems (Loranty and others, 2011). We have also shown that NDVI can successfully predict growing season GPP, R_{eco} and NEE of sub-Arctic heath and lichen communities. Finally, the comparatively low GPP/LAI observed in hummocks near the forest edge is consistent with a decreased productivity observed in transition zones between Arctic vegetation types and soil moisture constraints on plant assimilation.

Acknowledgements

Thanks to all the staff at the Kevo Subarctic Research Institute and to all the colleagues who collaborated in lab and fieldwork tasks, especially D. Sayer, T. August, K. Leslie and A. Robertson. Thanks to B. Fletcher, V. Sloan and G. Phoenix for their plant survey data and to T. Hill for the land classification map. We are grateful to P. Stoy and M. Williams for helpful comments on earlier versions of the manuscript and also to E. Rastetter for his feedback. This study was funded by NERC (UK) through the ABACUS consortium (Arctic Biosphere-Atmosphere Coupling at Multiple Scales, www.geos.ed.ac.uk/abacus; grant No. NE/D005760/1), within the framework of the International Polar Year (2007-2008). RP also benefited from a contract within the

573 MONTES project (CSD 2008-00040) and a ‘Juan de la Cierva’ fellowship, both funded
574 by the Spanish Ministry of Science and Innovation.

575

576 **References**

577 Alm J, Schulman L, Walden J, Nykänen H, Martikainen PJ, Silvola J. 1999. Carbon
578 balance of a boreal bog during a year with an exceptionally dry summer. Ecology 80:
579 161–174.

580 Alm J, Talanov A, Saarnio S, Silvola J, Ikkonen E, Aaltonen H, Nykänen H,
581 Martikainen PJ. 1997. Reconstruction of the carbon balance for microsites in a boreal
582 oligotrophic pine fen, Finland. Oecologia 110: 423–431.

583 Asner GP, Scurlock JMO, A. Hicke J. 2003. Global synthesis of leaf area index
584 observations: implications for ecological and remote sensing studies. Global Ecology
585 and Biogeography 12: 191–205.

586 Atkin OK, Bruhn D, Tjoelker MG. 2005. Response of Plant Respiration to Changes in
587 Temperature: Mechanisms and Consequences of Variations in Q_{10} Values and
588 Acclimation. In: Lambers H, Ribas-Carbó M, eds. Advances in Photosynthesis and
589 Respiration. Plant Respiration: From Cell to Ecosystem. Dordrecht, The Netherlands:
590 Springer, 95–135.

591 Beck PSA, Juday GP, Alix C, Barber VA, Winslow SE, Sousa EE, Heiser P, Herriges
592 JD, Goetz SJ. 2011. Changes in forest productivity across Alaska consistent with biome
593 shift. Ecology Letters 14:373–379.

594

595 Boelman NT, Stieglitz M, Griffin KL, Shaver GR. 2005. Inter-annual variability of
596 NDVI in response to long-term warming and fertilization in wet sedge and tussock
597 tundra. Oecologia 143: 588–597.

598 Boelman NT, Stieglitz M, Rueth HM, Sommerkorn M, Griffin KL, Shaver GR, Gamon
599 JA. 2003. Response of NDVI, biomass, and ecosystem gas exchange to long-term
600 warming and fertilization in wet sedge tundra. Oecologia 135: 414–421.

601 Bosiö J, Johansson M, Callaghan T, Johansen B, Christensen T. 2012. Future vegetation
602 changes in thawing subarctic mires and implications for greenhouse gas exchange—a
603 regional assessment. Climatic Change: 1–20.

604 Bubier J, Crill P, Mosedale A, Frolking S, Linder E. 2003. Peatland responses to
605 varying interannual moisture conditions as measured by automatic CO_2 chambers.
606 Global Biogeochemical Cycles 17: 1066.

607 Burrows EH, Bubier JL, Mosedale A, Cobb GW, Crill PM. 2005. Net Ecosystem
608 Exchange of Carbon dioxide in a Temperate Poor Fen: a Comparison of Automated and
609 Manual Chamber Techniques. Biogeochemistry 76: 21–45.

610 Cai T, Flanagan LB, Syed KH. 2010. Warmer and drier conditions stimulate respiration
611 more than photosynthesis in a boreal peatland ecosystem: Analysis of automatic
612 chambers and eddy covariance measurements. Plant, Cell & Environment 33: 394–407.

613 Christensen JH, Hewitson B, Busuioc A, Chen A, Gao X, Held I, Jones R, Kolli RK,
614 Kwon WT, Laprise R. 2007. Regional climate projections. In: Solomon S, Qin D,
615 Manning M, Chen Z, Marquis M, Averyt KB, Tignor M, Miller HL, eds. Climate
616 Change 2007: The Physical Science Basis. Contribution of Working Group I to the

Fourth Assessment Report of the Intergovernmental Panel on Climate Change. Cambridge, UK and New York, USA: Cambridge University Press, p847–940.

Dagg J, Lafleur P. 2010. An application of plot-scale NDVI in predicting carbon dioxide exchange and leaf area index in heterogeneous subarctic tundra. Canadian Journal of Remote Sensing 36: S111–S123.

Dagg J, Lafleur P. 2011. Vegetation Community, Foliar Nitrogen, and Temperature Effects on Tundra CO_2 Exchange across a Soil Moisture Gradient. Arctic, Antarctic, and Alpine Research 43: 189–197.

Dorrepaal E, Toet S, Van Logtestijn RSP, Swart E, Van de Weg MJ, Callaghan TV, Aerts R. 2009. Carbon respiration from subsurface peat accelerated by climate warming in the subarctic. Nature 460: 616–619.

Elmendorf SC, Henry GHR, Hollister RD, Björk RG, Boulanger-Lapointe N, Cooper EJ, Cornelissen JHC, Day TA, Dorrepaal E, Elumeeva TG, Gill M, Gould WA, Harte J, Hik DS, Hofgaard A, Johnson DR, Johnstone JF, Jónsdóttir IS, Jorgenson JC, Klanderud K, Klein JA, Koh S, Kudo G, Lara M, Lévesque E, Magnússon B, May JL, Mercado-Díaz JA, Michelsen A, Molau U, Myers-Smith IH, Oberbauer SF, Onipchenko VG, Rixen C, Schmidt NM, Shaver GR, Spasojevic MJ, Þórhallsdóttir ÞE, Tolvanen A, Troxler T, Tweedie CE, Villareal S, Wahren C-H, Walker X, Webber PJ, Welker JM, Wipf S. 2012. Plot-scale evidence of tundra vegetation change and links to recent summer warming. Nature Climate Change 2: 453–457.

Fletcher BJ, Gornall JL, Poyatos R, Press MC, Stoy PC, Huntley B, Baxter R, Phoenix GK. 2012. Photosynthesis and productivity in heterogeneous arctic tundra:

consequences for ecosystem function of mixing vegetation types at stand edges. Journal of Ecology 100: 441–451.

Heikkinen JEP, Virtanen T, Huttunen JT, Elsakov V, Martikainen PJ, others. 2004. Carbon balance in East European tundra. Global Biogeochemical Cycles 18: 1–14.

Heinemeyer A, Di Bene C, Lloyd AR, Tortorella D, Baxter R, Huntley B, Gelsomino A, Ineson P. 2011. Soil respiration: implications of the plant-soil continuum and respiration chamber collar-insertion depth on measurement and modelling of soil CO_2 efflux rates in three ecosystems. European Journal of Soil Science 62: 82–94.

Huemmrich K., Gamon JA, Tweedie CE, Oberbauer SF, Kinoshita G, Houston S, Kuchy A, Hollister RD, Kwon H, Mano M. 2010. Remote sensing of tundra gross ecosystem productivity and light use efficiency under varying temperature and moisture conditions. Remote Sensing of Environment 114: 481–489.

Humphreys ER, Lafleur PM, Flanagan LB, Hedstrom N, Syed KH, Glenn AJ, Granger R. 2006. Summer carbon dioxide and water vapor fluxes across a range of northern peatlands. Journal of Geophysical Research 111: G04011.

Johnson LC, Shaver GR, Giblin AE, Nadelhoffer KJ, Rastetter ER, Laundre JA, Murray GL. 1996. Effects of drainage and temperature on carbon balance of tussock tundra microcosms. Oecologia 108: 737–748.

Jones HG. 1992. Plants and microclimate: a quantitative approach to environmental plant physiology. Cambridge, UK.: Cambridge University Press. 428p.

659 Kulmala L, Pumpanen J, Hari P, Vesala T. 2011. Photosynthesis of ground vegetation
660 in different aged pine forests: Effect of environmental factors predicted with a process-
661 based model. Journal of Vegetation Science 22: 96–110.

662 Kulmala L, Pumpanen J, Vesala T, Hari P. 2009. Photosynthesis of boreal ground
663 vegetation after a forest clear-cut. Biogeosciences 6: 2495–2507.

664 Kutzbach L, Schneider J, Sachs T, Giebels M, Nykanen H, Shurpali NJ, Martikainen PJ,
665 Alm J, Wilmking M. 2007. CO_2 flux determination by closed-chamber methods can be
666 seriously biased by inappropriate application of linear regression. Biogeosciences 4:
667 1005–1025.

668 Larsen KS, Ibrom A, Beier C, Jonasson S, Michelsen A. 2007. Ecosystem respiration
669 depends strongly on photosynthesis in a temperate heath. Biogeochemistry 85: 201–
670 213.

671 Limpens J, Berendse F, Blodau C, Canadell JG, Freeman C, Holden J, Roulet N, Rydin
672 H, Schaepman-Strub G. 2008. Peatlands and the carbon cycle: from local processes to
673 global implications: a synthesis. Biogeosciences 5: 1475.

674 Lindroth A, Lund M, Nilsson M, Aurela M, Christensen TR, Laurila T, Rinne J, Riutta
675 T, Sagerfors J, Ström L. 2007. Environmental controls on the CO_2 exchange in north
676 European mires. Tellus B 59: 812–825.

677 Loranty MM, Goetz SJ, Rastetter EB, Rocha AV, Shaver GR, Humphreys ER, Lafleur
678 PM. 2011. Scaling an Instantaneous Model of Tundra NEE to the Arctic Landscape.
679 Ecosystems 14: 76–93.

680 Lund M, Lafleur PM, Roulet NT, Lindroth A, Christensen TR, Aurela M, Chojnicki
681 BH, Flanagan LB, Humphreys ER, Laurila T. 2010. Variability in exchange of CO_2
682 across 12 northern peatland and tundra sites. Global Change Biology 16: 2436–2448.

683 Maanavilja L, Riutta T, Aurela M, Pulkkinen M, Laurila T, Tuittila E-S. 2011. Spatial
684 variation in CO_2 exchange at a northern aapa mire. Biogeochemistry 104: 325–345.

685 Mahecha MD, Reichstein M, Carvalhais N, Lasslop G, Lange H, Seneviratne SI, Vargas
686 R, Ammann C, Arain MA, Cescatti A, Janssens IA, Migliavacca M, Montagnani L
687 Richardson, AD. 2010. Global Convergence in the Temperature Sensitivity of
688 Respiration at Ecosystem Level. Science 329: 838–840.

689 Marushchak ME, Kiepe I, Biasi C, Elsakov V, Friborg T, Johansson T, Soegaard H,
690 Virtanen T, Martikainen PJ. 2013. Carbon dioxide balance of subarctic tundra from plot
691 to regional scales. Biogeosciences 10: 437–452.

692 McMichael CE. 1999. Estimating CO_2 exchange at two sites in Arctic tundra
693 ecosystems during the growing season using a spectral vegetation index. International
694 Journal of Remote Sensing 20: 683–698.

695 Moore TR, Bubier JL, Frolking SE, Lafleur PM, Roulet NT. 2002. Plant biomass and
696 production and CO_2 exchange in an ombrotrophic bog. Journal of Ecology 90: 25–36.

697 Natali SM, Schuur EAG, Rubin RL. 2012. Increased plant productivity in Alaskan
698 tundra as a result of experimental warming of soil and permafrost. Journal of Ecology
699 100: 488–498.

700 Nobrega S, Grogan P. 2008. Landscape and Ecosystem-Level Controls on Net Carbon
701 Dioxide Exchange along a Natural Moisture Gradient in Canadian Low Arctic Tundra.
702 Ecosystems 11: 377–396.

703 Oberbauer SF, Tweedie CE, Welker JM, Fahnestock JT, Henry GHR, Webber PJ,
704 Hollister RD, Walker MD, Kuchy A, Elmore E. 2007. Tundra CO_2 fluxes in response to
705 experimental warming across latitudinal and moisture gradients. Ecological
706 Monographs 77: 221–238.

707 Oechel WC, Vourlitis GL, Brooks S, Crawford TL, Dumas E. 1998. Intercomparison
708 among chamber, tower, and aircraft net CO_2 and energy fluxes measured during the
709 Arctic System Science Land-Atmosphere-Ice Interactions (ARCSS-LAII) Flux Study.
710 Journal of Geophysical Research-Atmospheres 103: 28993–29003.

711 Pelletier L, Garneau M, Moore T. 2011. Variation in CO_2 exchange over three summers
712 at microform scale in a boreal bog, Eastmain region, Québec, Canada. Journal of
713 Geophysical Research-Biogeosciences 116: G03019.

714 Pinheiro JC, Bates DM. 2000. Mixed-effects models in S and S-PLUS. Springer Verlag.
715 528p.

716 La Puma IP, Philippi TE, Oberbauer SF. 2007. Relating NDVI to ecosystem CO_2
717 exchange patterns in response to season length and soil warming manipulations in arctic
718 Alaska. Remote Sensing of Environment 109: 225–236.

719 R Development Core Team. 2009. R: A Language and Environment for Statistical
720 Computing. R Foundation for Statistical Computing,Vienna, Austria.

721 Riutta T, Laine J, Aurela M, Rinne J, Vesala T, Laurila T, Haapanala S, Pihlatie M,
722 Tuittila E-S. 2007. Spatial variation in plant community functions regulates carbon gas
723 dynamics in a boreal fen ecosystem. Tellus B 59: 838–852.

724 Schuur EAG, Vogel JG, Crummer KG, Lee H, Sickman JO, Osterkamp TE. 2009. The
725 effect of permafrost thaw on old carbon release and net carbon exchange from tundra.
726 Nature 459: 556–559.

727 Shaver GR, Street LE, Rastetter EB, Van Wijk MT, Williams M. 2007. Functional
728 convergence in regulation of net CO_2 flux in heterogeneous tundra landscapes in Alaska
729 and Sweden. Journal of Ecology 95: 802–817.

730 Soegaard H, Nordstroem C, Friborg T, Hansen BU, Christensen TR, Bay C. 2000.
731 Trace gas exchange in a high-Arctic valley: 3. Integrating and scaling CO_2 fluxes from
732 canopy to landscape using flux data, footprint modeling, and remote sensing. Global
733 Biogeochemical Cycles 14: 725–744.

734 Spadavecchia L, Williams M, Bell R, Stoy PC, Huntley B, Van Wijk MT. 2008.
735 Topographic controls on the leaf area index and plant functional type of a tundra
736 ecosystem. Journal of Ecology 96: 1238–1251.

737 Stoy PC, Williams M, Evans JG, Prieto-Blanco A, Disney M, Hill TC, Wade TJ, Street
738 LE. Upscaling tundra CO_2 exchange from chamber to eddy covariance tower. Arctic,
739 Antarctic, and Alpine Research 45: 275-284.

740 Street LE, Shaver GR, Williams M, Van Wijk MT. 2007. What is the relationship
741 between changes in canopy leaf area and changes in photosynthetic CO_2 flux in arctic
742 ecosystems? Journal of Ecology 95: 139–150.

743 Street LE, Stoy PC, Sommerkorn M, Fletcher BJ, Sloan VL, Hill TC, Williams M.
744 2012. Seasonal bryophyte productivity in the sub-Arctic: a comparison with vascular
745 plants. Functional Ecology 26: 365–378.

746 Subke J-A, Heinemeyer A, Vallack H, Leronni V, Baxter R, Ineson P. 2012. Fast
747 assimilate turnover revealed by in situ $^{13}CO_2$ pulse-labelling in Subarctic tundra. Polar
748 Biology 35: 1209–1219.

749 Turunen J, Tomppo E, Tolonen K, Reinikainen A. 2002. Estimating carbon
750 accumulation rates of undrained mires in Finland – application to boreal and subarctic
751 regions. The Holocene 12: 69–80.

752 Van Vliet-Lanoe B, Seppala M. 2002. Stratigraphy, age and formation of peaty earth
753 hummocks (pounus), Finnish Lapland. The Holocene 12: 187–199.

754 Wayolle AAJ. 2011. Multiscale Soil Carbon Distribution in Two Sub-Arctic
755 Landscapes.PhD dissertation, University of Stirling, Stirling, UK.

756 Van Wijk MT, Williams M, Shaver GR. 2005. Tight coupling between leaf area index
757 and foliage N content in arctic plant communities. Oecologia 142: 421–427.

758 Williams M, Street LE, Wijk MT, Shaver GR. 2006. Identifying Differences in Carbon
759 Exchange among Arctic Ecosystem Types. Ecosystems 9: 288–304.

760 Wohlfahrt G, Pilloni S, Hörtnagl L, Hammerle A. 2010. Estimating carbon dioxide
761 fluxes from temperate mountain grasslands using broad-band vegetation indices.
762 Biogeosciences 7: 683–694.

763

764 **Table legends**

765 Table 1. Vegetation characteristics of the study plots: percent cover of the dominant
766 species, total percent cover of vascular species, biomass and leaf area index (LAI) of
767 vascular plants and maximum patch-scale normalised differential vegetation index
768 (NDVI).

769 Table 2. Summary statistics for the relationships among NEE model parameters,
770 vegetation parameters and cumulative CO_2 fluxes, depicted in Figures 5, 7 and 8.

771 Table 3. Statistics for mixed models of NEE model parameters as a function of
772 environmental and vegetation variables. The response variable was log-transformed
773 when needed. Vegetation type HM has been considered the reference level. Rows in
774 bold show statistically significant effects ($P < 0.05$) and underlined results depict
775 marginally significant effects ($0.1 < P < 0.05$).

776 Table 4. Growing season cumulative values of CO_2-C fluxes per ground area (g C m^{-2})
777 and expressed per unit leaf area for the studied vegetation types. Different letters
778 indicate significant ($P < 0.05$) differences among types. Marginal differences ($0.1 < P$
779 < 0.05) between two vegetation types are also underlined.

780

Table 1.

Plot	Vegetation Type	Species	Vascular % cover	Non-vascular % cover	Vascular Biomass (g m^{-2})	Vascular LAI m^2 m^{-2}	$NDVI_{max}$
HM1	Mire hummock	*Empetrum nigrum* (25) *Rubus chamaemorus* (6) *Sphagnum* spp. (11)	41	11	82.9	0.37	0.65
HM2	Mire hummock	*Empetrum nigrum* (48) *Vaccinium uliginosum* (3)	53	5	228.7	0.94	0.72
HM3	Mire hummock	*Empetrum nigrum* (31) *Vaccinium vitis-idaea* (11) *Pleurozium schreberi* (12)	52	15	42.6	0.27	0.69
HF1	Forest hummock	*Empetrum nigrum* (24) *Vaccinium vitis-idaea* (21) *Sphagnum* spp. (11)	49	23	107.9	0.63	0.69
HF2	Forest hummock	*Empetrum nigrum* (38) *Vaccinium vitis-idaea* (14)	52	7	248.8	1.22	0.78
HF3	Forest hummock	*Empetrum nigrum* (51) *Vaccinium myrtillus* (14) Lichen (10)	75	10	393.9	2.07	0.85
HL1	Eroded hummock	Lichen (17)	0	17	0	0	0.46
HL2	Eroded hummock	Lichen (15) Acrocarpous moss (28)	0	43	0	0	0.41
HL3	Eroded hummock	Lichen (25) Acrocarpous moss (17)	5	44	0	0	0.41
DH1	Dry hollow	*Calluna vulgaris* (40) *Vaccinium uliginosum* (10)	52	13	295.5	0.85	0.79
DH2	Dry hollow	*Calluna vulgaris* (20)	26	8	62.8	0.18	0.65

DH3	Dry hollow	*Vaccinium myrtillus* (3) *Calluna vulgaris* (51) *Vaccinium uliginosum* (2)	58	3	144.0	0.40	0.67

Table 2.

Response variable	Explanatory variable	Intercept	Slope	R^2
NEE model parameters				
ln(Maximum P_{600})	ln(Maximum NDVI)	3.56±0.14	3.06±0.27	0.92
ln(Maximum R_0)	ln(Maximum NDVI)	1.83±0.16	1.69±0.31	0.73
Vegetation parameters				
Vascular biomass	Maximum NDVI	-10003.4±164.1	1638.2±226.5	0.87
Vascular LAI	Maximum NDVI	-5.00±0.92	8.00±1.27	0.83
Cumulative CO_2 fluxes				
NEE	Maximum NDVI	316.8±86.48	-564.73±130.46	0.62
ln(-GPP)	ln(Maximum NDVI)	6.81±0.11	3.12±0.22	0.95
R_{eco}	Maximum NDVI	-56.29±44.71	427.80±67.44	0.78
NEE	LAI	-20.80±40.00	-87.18±41.94	0.29
GPP	LAI	-241.03±37.92	-126.72±39.76	0.53
log(R_{eco})	ln(LAI)	5.61±0.05	0.17±0.06	0.51
ln(R_{eco})	ln(-GPP)	3.00±0.39	0.44±0.07	0.76

Table 3.

Response variable	Fixed effect	Estimate	SE	df	t	*P*-value	AIC	R^2
log(P_{600})	**(Intercept)**	**-1.446**	**0.402**	**218**	**-3.594**	**0.0004**	124.29	0.88
	NDVI	**1.522**	**0.387**	**218**	**3.932**	**0.0001**		
	T_0	**0.199**	**0.029**	**218**	**6.885**	**0.0000**		
	T_0^2	**-0.005**	**0.001**	**218**	**-3.954**	**0.0001**		
	VPD	**-0.510**	**0.223**	**218**	**-2.287**	**0.0232**		
	Vegtype: HF	-0.216	0.221	8	-0.977	0.3571		
	Vegtype: DH	-0.137	0.216	8	-0.636	0.5425		
	Vegtype: HL	-1.442	0.231	8	-6.234	0.0002		
	DOY	**0.007**	**0.001**	**218**	**5.262**	**0.0000**		
log(α)	**(Intercept)**	**-0.069**	**0.014**	**235**	**-4.909**	**0.0000**	-1261.98	0.41
	NDVI	**0.066**	**0.013**	**235**	**5.048**	**0.0000**		
	T_0	**0.002**	**0.000**	**235**	**5.092**	**0.0000**		
	DOY	**0.000**	**0.000**	**235**	**4.232**	**0.0000**		
log(R_0)	**(Intercept)**	**3.211**	**1.250**	**220**	**2.569**	**0.0109**	359.05	0.50
	NDVI	0.904	0.511	220	1.769	0.0782		
	Vegtype: HF	**-2.566**	**0.803**	**8**	**-3.195**	**0.0127**		
	Vegtype: DH	**-1.726**	**0.533**	**8**	**-3.238**	**0.0119**		
	Vegtype: HL	**-2.567**	**0.625**	**8**	**-4.109**	**0.0034**		
	T_0	**0.036**	**0.009**	**220**	**4.066**	**0.0001**		
	SWC	**-5.667**	**1.617**	**220**	**-3.505**	**0.0006**		
Q_{10}	**(Intercept)**	**2.880**	**0.421**	**237**	**6.849**	**0.0000**	650.19	0.03
	DOY	**-0.006**	**0.002**	**237**	**-2.911**	**0.0039**		

Table 4.

	Vegetation Type			
	HM	HF	DH	HL
NEE	-92.7±10.6[a]	-82.3±86.1[a]	-84.6±40.2[a]	66.1±23.8[a]
GPP	-331.1±14.7[a]	-369.3±80.1[a]	-312.3±73.2[a]	-61.1±4.9[b]
R_{eco}	239.6±6.1[a]	287.2±12.2[a]	227.4±33.2[ab]	126.1±26.4[b]
NEE/LAI	-246.7±97.6[a]	-28.12±57.8 [a]	-162.7±35.2 [a]	na
GPP/LAI	-833.5±279.9[a]	-307.6±38.1[a]	-778.4±149.8[a]	na
R_{eco}/LAI	594.5±186.9[a]	280.1±95.5[a]	175.4±95.5[a]	na

781 **Figure legends**

782 Figure 1. Seasonal course of daily aggregates of environmental variables: a) mean site
783 air temperature b) Photosynthetically Active Radiation (PAR), c) precipitation and d)
784 volumetric soil content (0-10 cm) measured in a representative plot of each vegetation
785 type. Panel a) also shows hourly variation in air temperature in grey.

786 Figure 2. Time series of hourly Net Ecosystem CO_2 Exchange (NEE) measured in three
787 replicated chambers in a) mire hummocks (HM), b) forest hummocks (HF), c) dry
788 hollows (DH) and d) lichen-covered hummocks (HL).

789 Figure 3. Diel courses of NEE during the growing season: DOY 170, DOY 195, DOY
790 220 and DOY 254.Lines depict hourly NEE for three replicated chambers in mire
791 hummocks (HM, 1st row), forest hummocks (HF, 2nd row), dry hollows (DH, 3rd row)
792 and lichen-covered hummocks (HL, 4th row).

793 Figure 4. Seasonal course of NEE model parameters for all measured chambers,
794 according to vegetation type: mire hummocks (HM, 1st column), forest hummocks (HF,
795 2nd column), dry hollows (DH, 3rd column) and lichen-covered hummocks (HL, 4th
796 column).

797 Figure 5. Relationships between maximum NDVI and: maximum values of (a) P_{600} and
798 (b) R_o, (c) plot vascular biomass and (d) plot LAI.

799 Figure 6. Growing season cumulative NEE (a), GPP (b) and R_{eco} (c) for all measured
800 plots.

801 Figure 7. Relationships between growing season cumulative NEE, GPP and R_{eco} and
802 either maximum NDVI (a, b, c) or plot LAI (d, e, f).

803 Figure 8. Relationship between growing season cumulative GPP and R_{eco}.

804

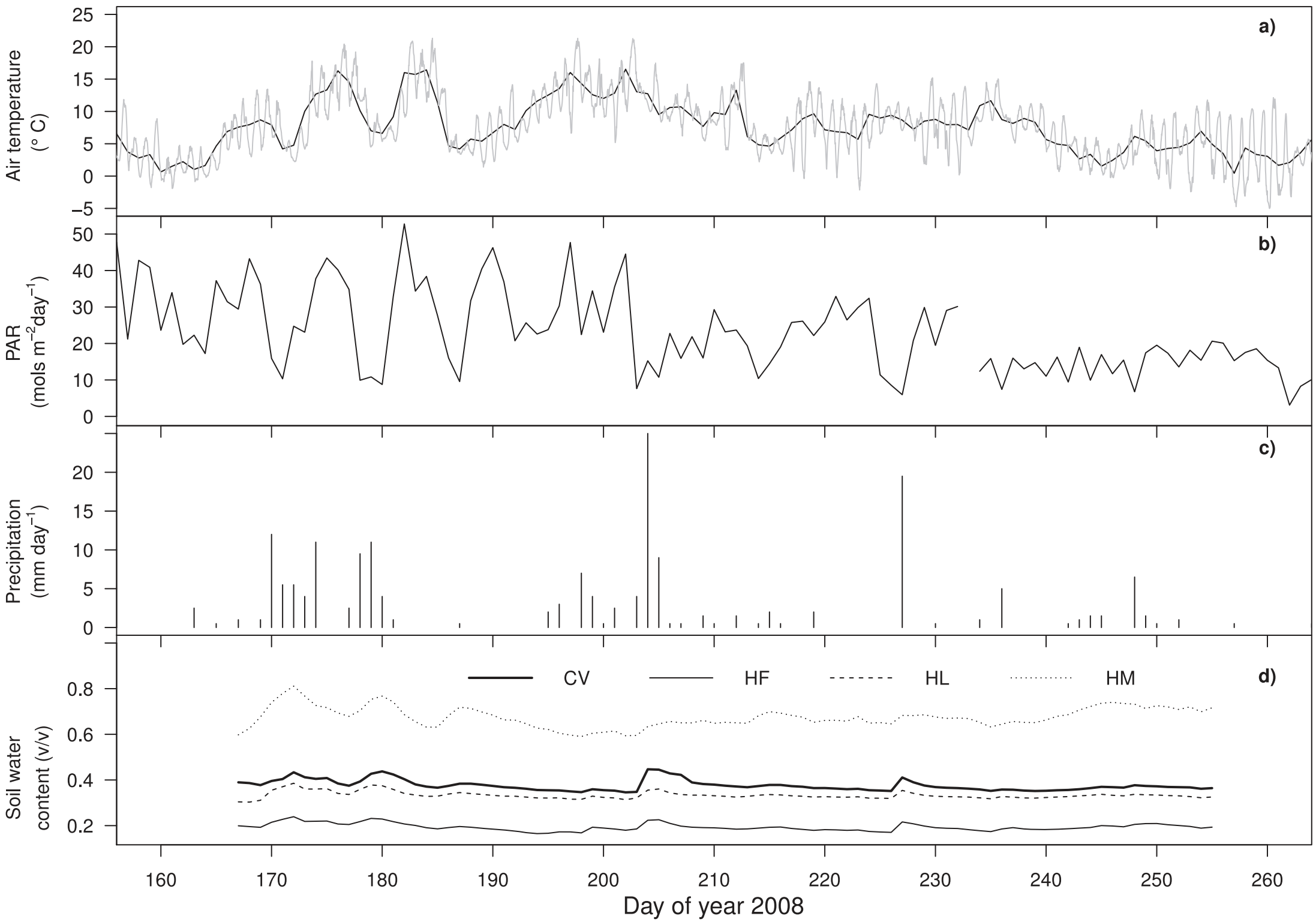
a)
Air temperature
(° C)
25
20
15
10
5
0
−5
b)
PAR
(mols m^{-2}day^{-1})
50
40
30
20
10
0
c)
Precipitation
(mm day^{-1})
20
15
10
5
0
d)
CV
HF
HL
HM
Soil water
content (v/v)
0.8
0.6
0.4
0.2
160
170
180
190
200
210
220
230
240
250
260
Day of year 2008

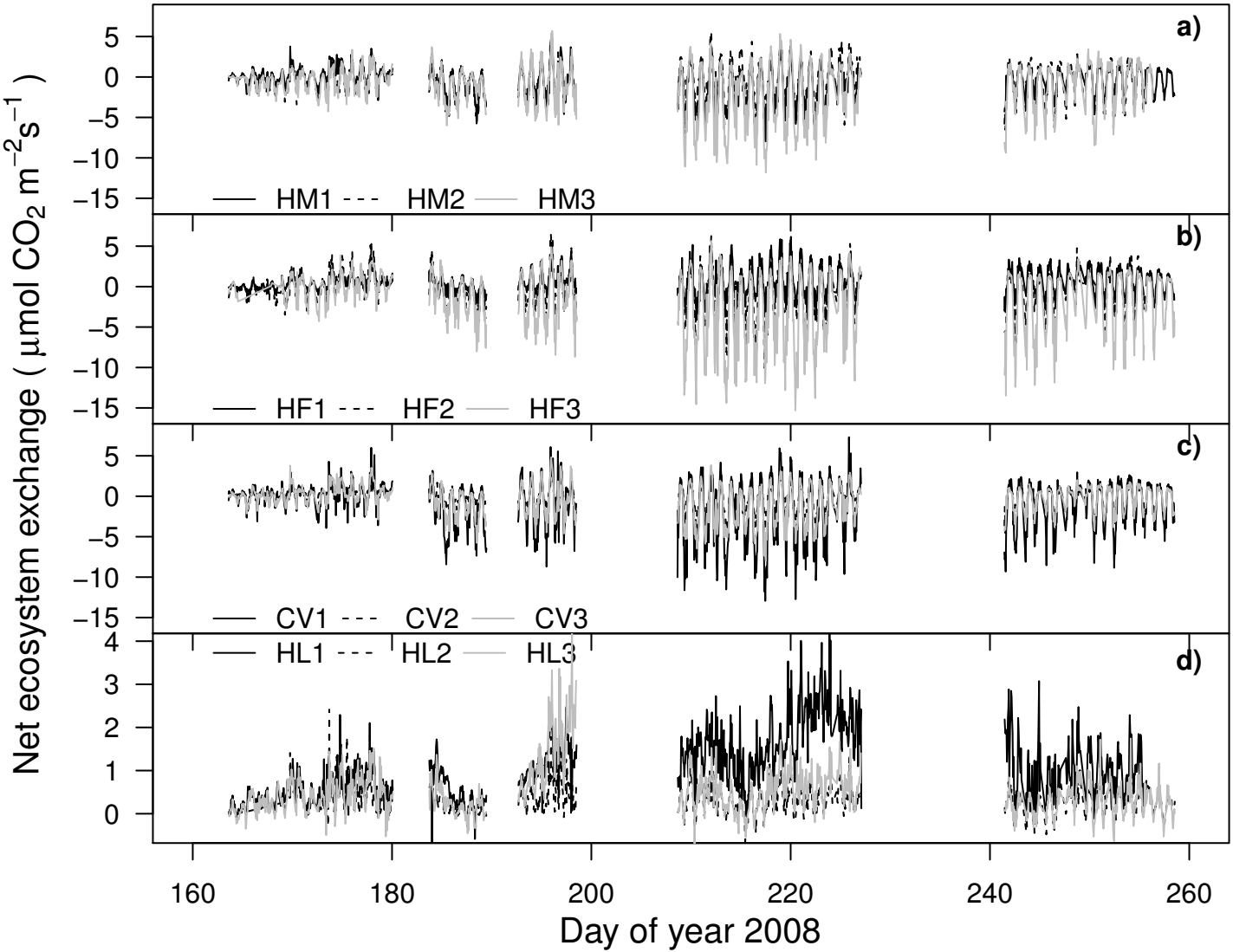
a)
b)
c)
d)
HM1
HM2
HM3
HF1
HF2
HF3
CV1
CV2
CV3
HL1
HL2
HL3
Net ecosystem exchange (µmol CO2 m−2s−1)
Day of year 2008
160
180
200
220
240
260

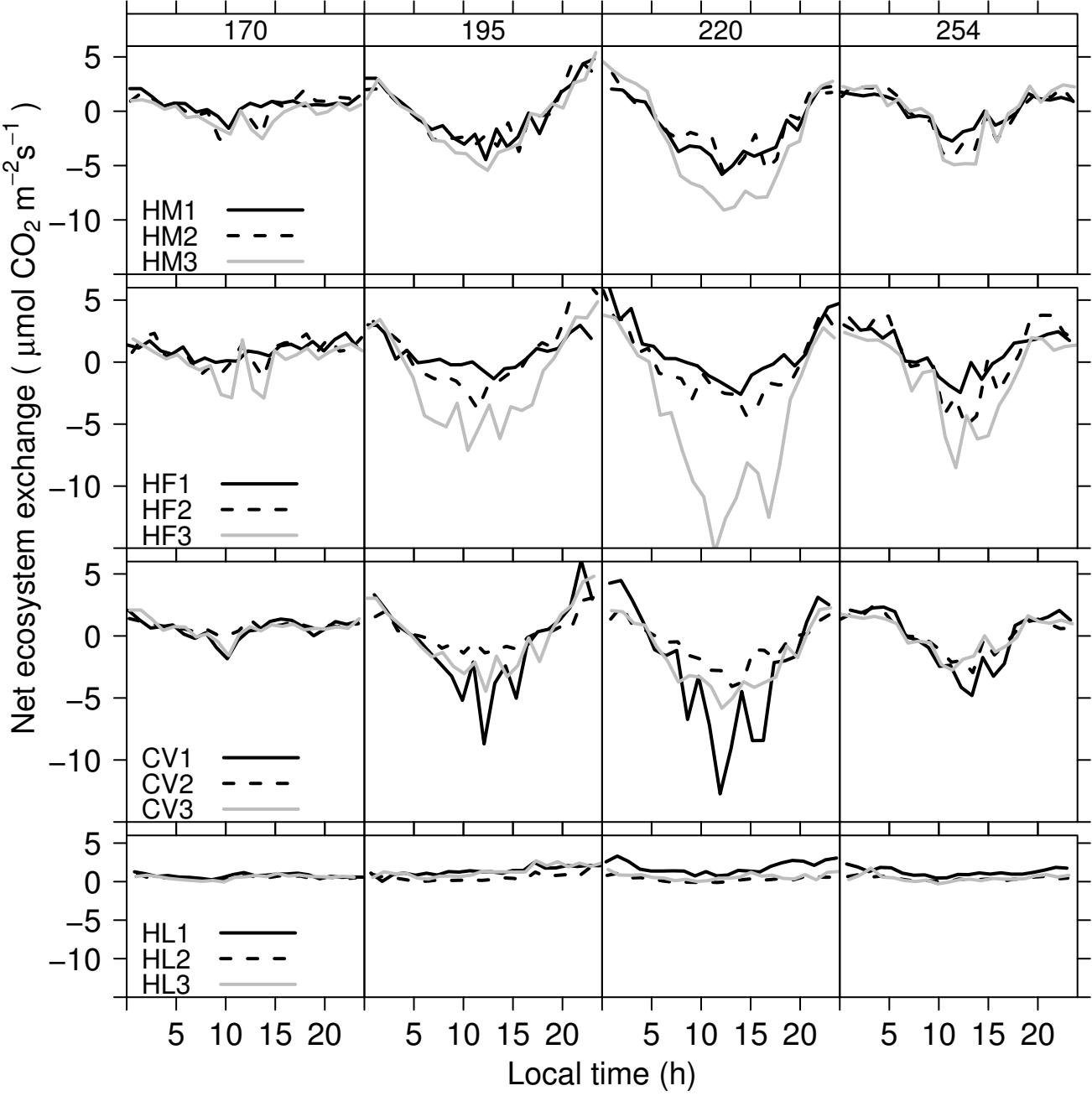
170
195
220
254
Net ecosystem exchange (µmol CO_2 $m^{-2}s^{-1}$)
5
0
−5
−10
HM1
HM2
HM3
HF1
HF2
HF3
CV1
CV2
CV3
HL1
HL2
HL3
5
10
15
20
Local time (h)

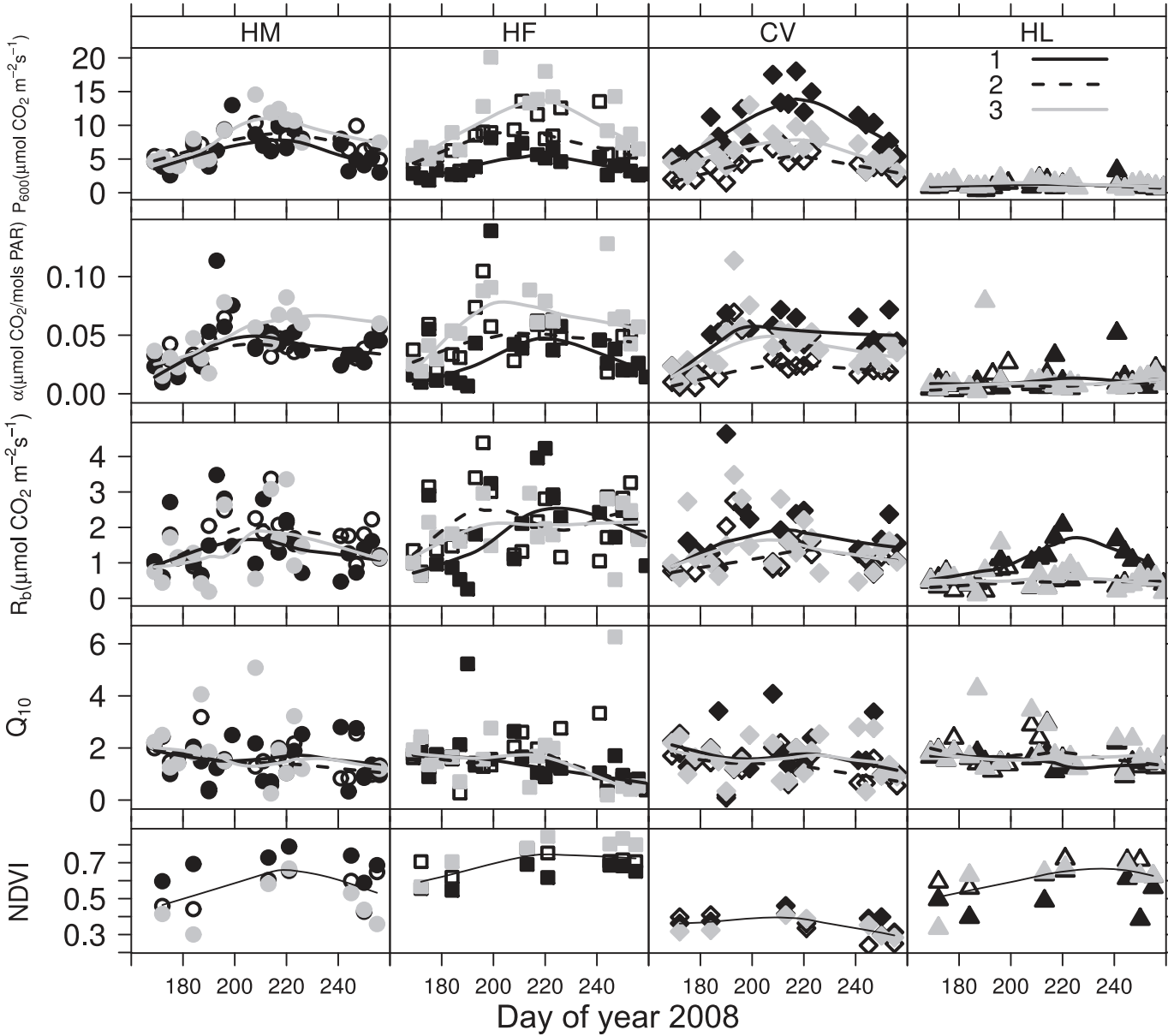
HM
HF
CV
HL
1
2
3
P_{600}(μmol CO_2 $m^{-2}s^{-1}$)
α(μmol CO_2/mols PAR)
R_b(μmol CO_2 $m^{-2}s^{-1}$)
Q_{10}
NDVI
Day of year 2008

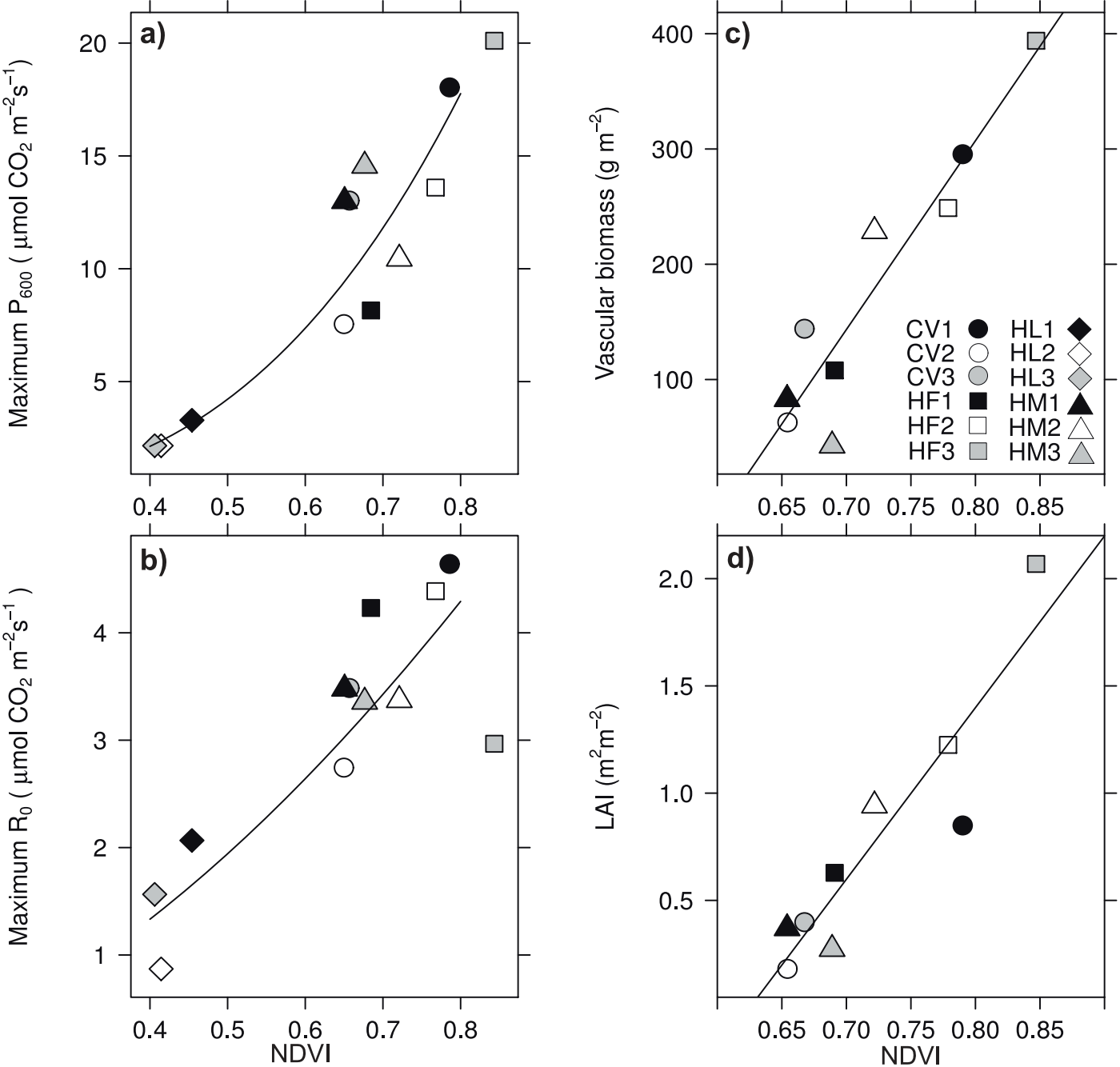
a)
b)
c)
d)
Maximum P_{600} (µmol CO_2 $m^{-2}s^{-1}$)
Maximum R_0 (µmol CO_2 $m^{-2}s^{-1}$)
Vascular biomass (g m^{-2})
LAI (m^2m^{-2})
NDVI
NDVI
CV1
CV2
CV3
HF1
HF2
HF3
HL1
HL2
HL3
HM1
HM2
HM3

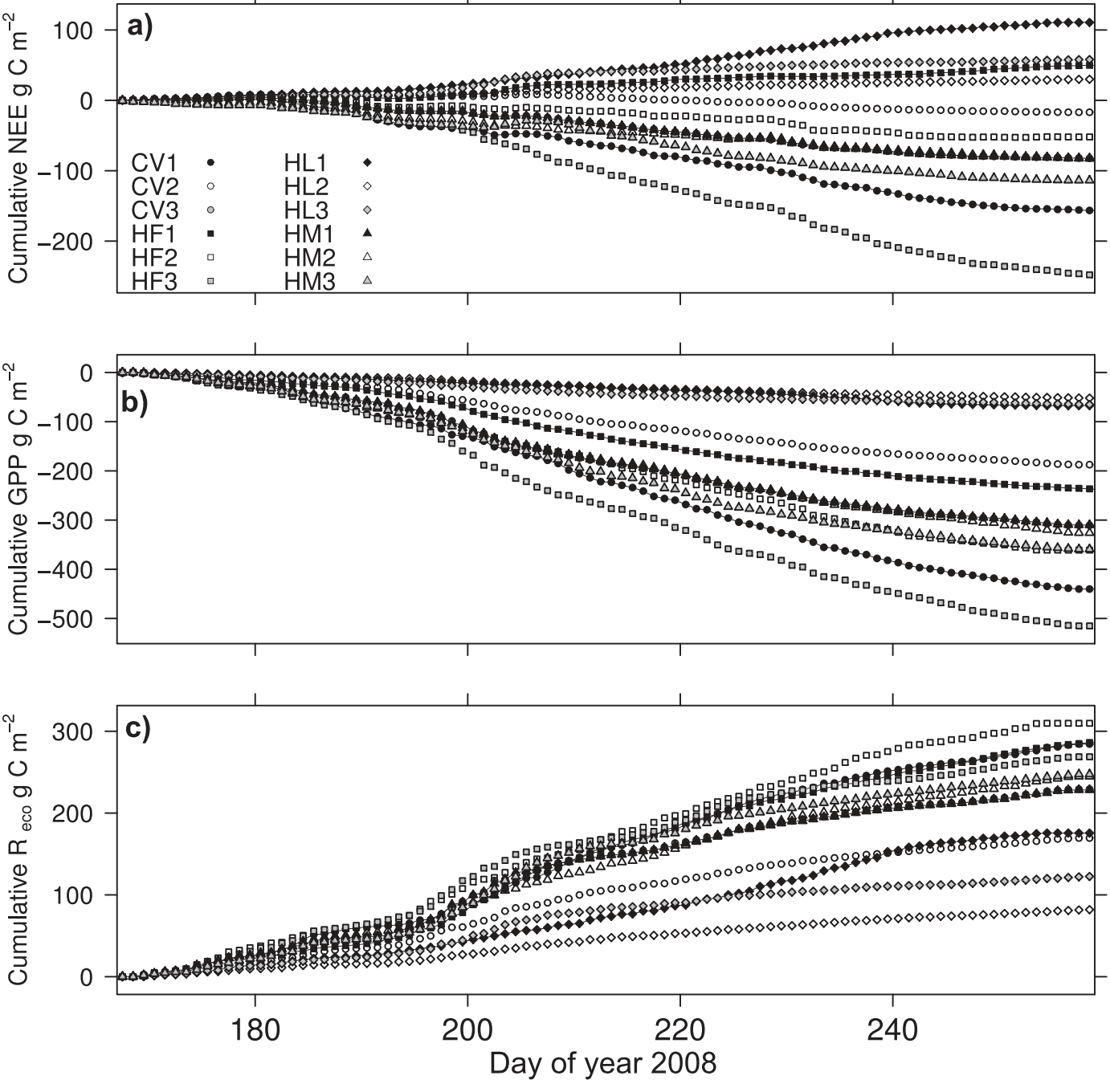
a)
b)
c)
Cumulative NEE g C m^{-2}
Cumulative GPP g C m^{-2}
Cumulative R$_{eco}$ g C m^{-2}
CV1
CV2
CV3
HF1
HF2
HF3
HL1
HL2
HL3
HM1
HM2
HM3
100
0
−100
−200
−300
−400
−500
300
200
180
220
240
Day of year 2008

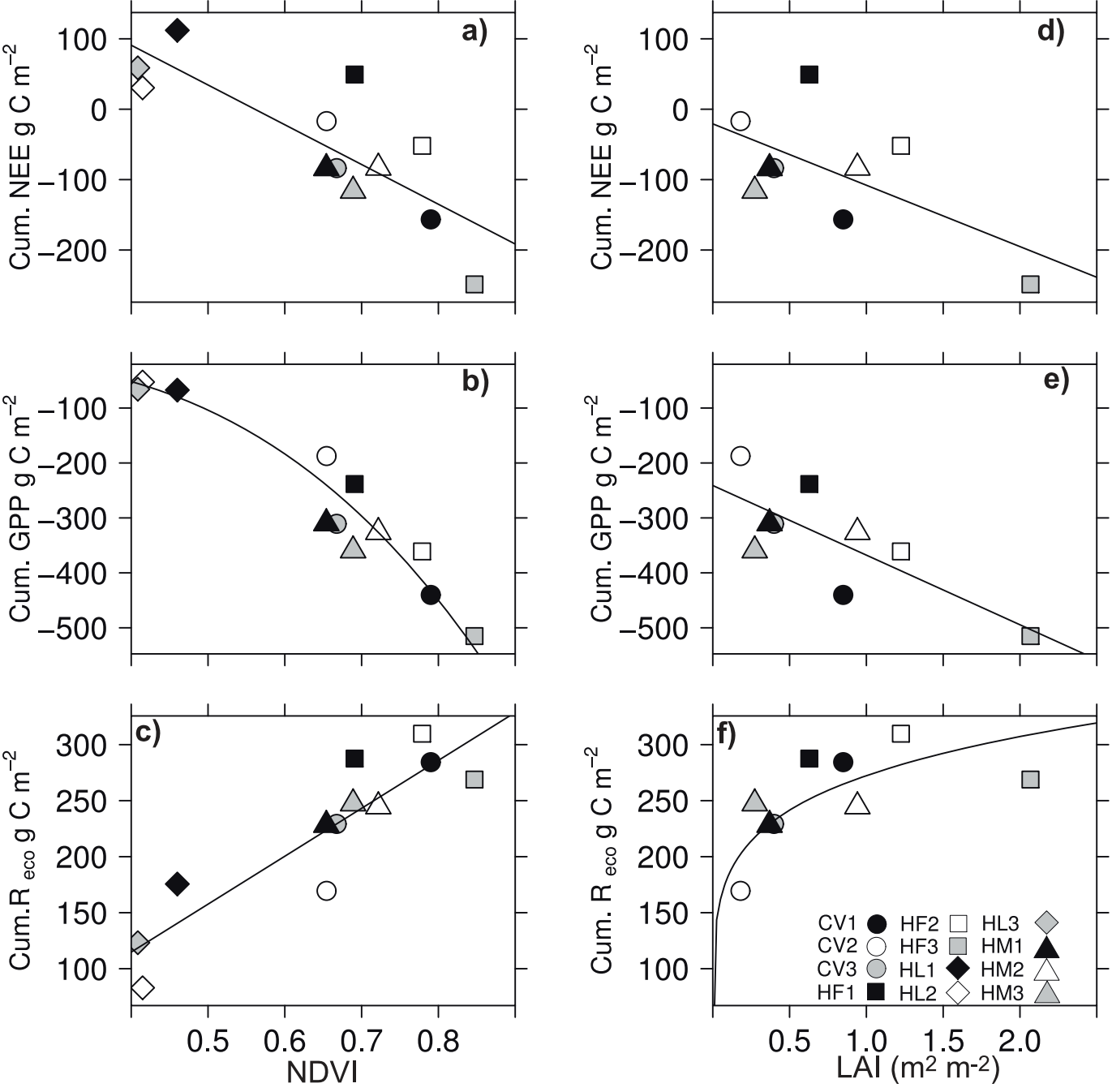
a)
d)
b)
e)
c)
f)
Cum. NEE g C m^{-2}
Cum. GPP g C m^{-2}
Cum.R$_{eco}$ g C m^{-2}
NDVI
LAI (m^2 m^{-2})
CV1
CV2
CV3
HF1
HF2
HF3
HL1
HL2
HL3
HM1
HM2
HM3

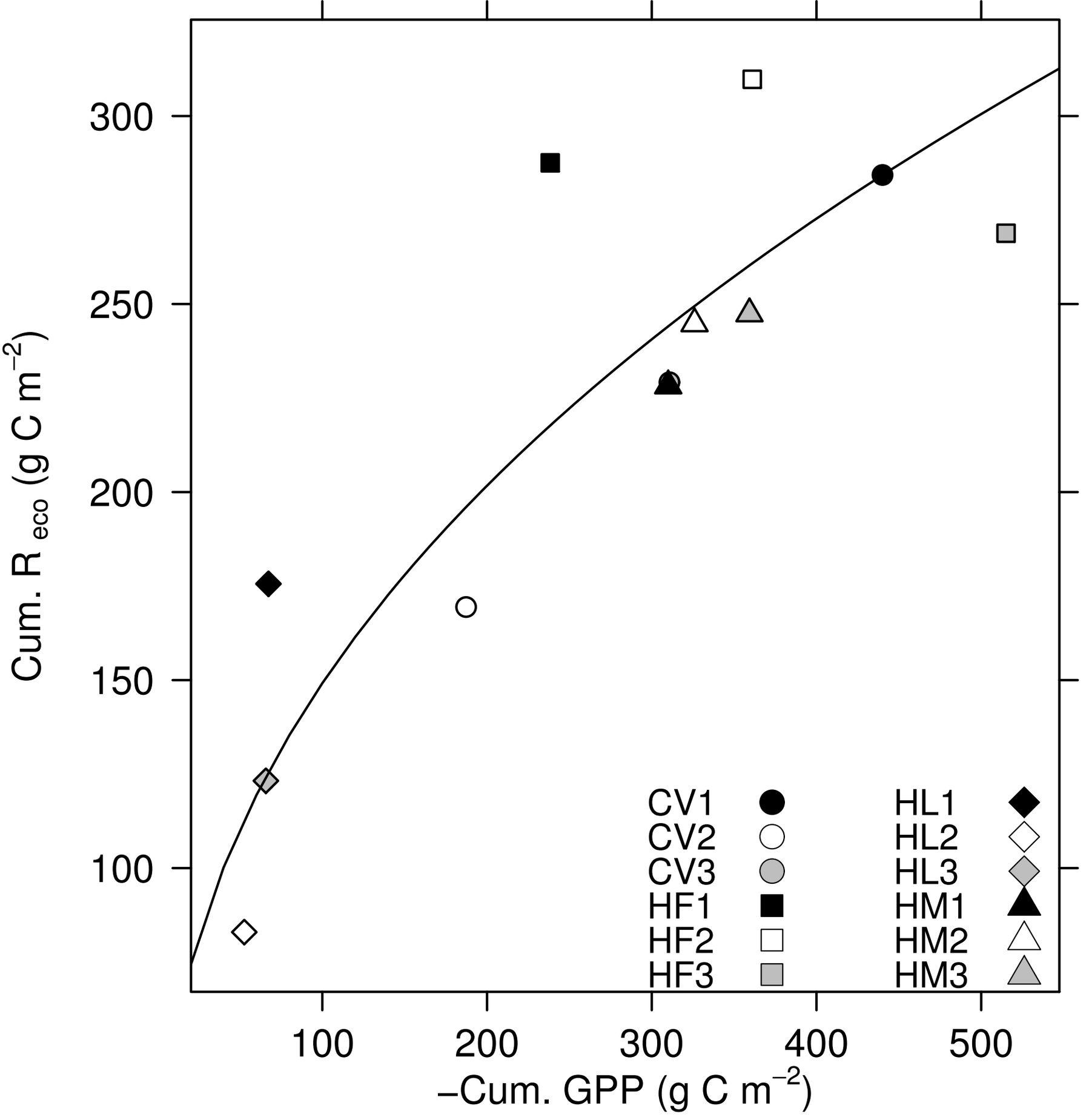
300
250
200
150
100
Cum. R eco (g C m−2)
100
200
300
400
500
–Cum. GPP (g C m−2)
CV1
CV2
CV3
HF1
HF2
HF3
HL1
HL2
HL3
HM1
HM2
HM3

Appendices

Appendix 1. Land classification map of the Petsikko field site, showing plot locations within the forest-mire ecotone (cf. Table 1 for the meaning of plot codes). The map is based on aerial photography taken in summer 2008 (T. Hill, unpublished). Coordinates are in UTM projection, zone 35N, datum WGS84.

Appendix 2. Statistics of the NEE model (DOY is day of year 2008). R_0 is basal respiration, β is respiration sensitivity to temperature, P_{max} is asymptotic maximum photosynthesis, α is quantum efficiency and P_{600} is gross photosynthesis at PAR = 600 µmol m^{-2} s^{-1}. Adjusted R^2 and root mean square error (RMSE) are also shown.